PNNL-25163

Pacific Northwest
NATIONAL LABORATORY

Proudly Operated by Battelle Since 1965

Predictive Engineering Tools for Injection-Molded Long-Carbon-Fiber Thermoplastic Composites

January 2016

Ba Nghiep Nguyen, Leonard S. Fifield
Pacific Northwest National Laboratory, Richland, WA 99354

Gregory Lambert, Donald G. Baird
Virginia Polytechnic and State University, Blacksburg, Virginia 24061

Jin Wang, Franco Costa
Autodesk, Inc., Ithaca, NY 14850

Charles L. Tucker III
University of Illinois at Urbana-Champaign, Urbana, IL 61801

Umesh N. Gandhi
Toyota Research Institute North America, Ann Arbor, MI 48105

Steven Mori
MAGNA Exteriors and Interiors Corporation, Aurora, Ontario, Canada

Eric J. Wollan, Dale Roland
PlastiComp, Inc., Winona, MN 55987

Project period: From October 1st 2012 to September 30th, 2016
Reporting period end date: December 31st, 2015
Quarterly report submitted to:
Aaron Yocum, National Energy Technology Laboratory, Morgantown, WV 26507

U.S. DEPARTMENT OF ENERGY

Prepared for the U.S. Department of Energy
under Contract **DE-AC05-76RL01830**

PACIFIC NORTHWEST NATIONAL LABORATORY
operated by
BATTELLE
for the
UNITED STATES DEPARTMENT OF ENERGY
under Contract DE-AC05-76RL01830

Printed in the United States of America

Available to DOE and DOE contractors from the
Office of Scientific and Technical Information,
P.O. Box 62, Oak Ridge, TN 37831-0062;
ph: (865) 576-8401
fax: (865) 576-5728
email: reports@adonis.osti.gov

Available to the public from the National Technical Information Service,
U.S. Department of Commerce, 5285 Port Royal Rd., Springfield, VA 22161
ph: (800) 553-6847
fax: (703) 605-6900
email: orders@ntis.fedworld.gov
online ordering: http://www.ntis.gov/ordering.htm

This document was printed on recycled paper.
(9/2003)

Predictive Engineering Tools for Injection-molded Long-Carbon-Fiber Thermoplastic Composites

Ba Nghiep Nguyen, Leonard S. Fifield
Pacific Northwest National Laboratory, Richland, WA 99354
Gregory Lambert, Donald G. Baird
Virginia Polytechnic and State University, Blacksburg, Virginia 24061
Jin Wang, Franco Costa
Autodesk, Inc., Ithaca, NY 14850
Charles L. Tucker III
University of Illinois at Urbana-Champaign, Urbana, IL 61801
Umesh N. Gandhi
Toyota Research Institute North America, Ann Arbor, MI 48105
Steven Mori
MAGNA Exteriors and Interiors Corporation, Aurora, Ontario, Canada
Eric J. Wollan, Dale Roland
PlastiComp, Inc., Winona, MN 55987

January 2016

Project period: From October 1st 2012 to September 30th, 2016
Reporting period end date: December 31st, 2015

Quarterly report submitted to:
Aaron Yocum, National Energy Technology Laboratory, Morgantown, WV 26507

Prepared for
the U.S. Department of Energy
under Contract DE-AC05-76RL01830

Pacific Northwest National Laboratory
Richland, Washington 99352

1. Objective

The objective of this project is to advance *predictive engineering (PE) tools* to accurately predict *fiber orientation and length distributions* in *injection-molded long-carbon fiber thermoplastic composites* for optimum design of automotive structures using these materials *to meet weight and cost reduction requirements* defined in Table 2 of DE-FOA-0000648 (Area of Interest 1).

2. Background

This project proposes to integrate, optimize and validate the fiber orientation and length distribution models previously developed and implemented in the Autodesk Simulation Moldflow Insight (ASMI) package for injection-molded long-carbon-fiber thermoplastic composites into a cohesive prediction capability. In our previous US Department of Energy (DOE) funded project, entitled *"Engineering Property Prediction Tools for Tailored Polymer Composite Structures,"* Pacific Northwest National Laboratory (PNNL), with the University of Illinois and Autodesk, Inc., developed a unique assembly of computational algorithms providing state-of-the-art process and constitutive models that enhance the capabilities of commercial software packages to predict fiber orientation and length distributions as well as subsequent mechanical properties of injection-molded long-fiber thermoplastic (LFT) composites. These predictive capabilities were validated using fiber analysis data generated at Oak Ridge National Laboratory on two-dimensional (2D) structures consisting of edge-gated plaques and center-gated disks injection-molded from long-glass-fiber/polypropylene (PP) and long-glass-fiber/polyamide 6,6 (PA66) pellets. The present effort aims at rendering the developed models more robust and efficient to automotive industry part design to enable weight savings and cost reduction. This ultimate goal will be achieved by optimizing the developed models, improving and integrating their implementations in ASMI, and validating them for a complex three-dimensional (3D) long-carbon fiber (LCF) thermoplastic automotive part. Both PP and PA66 are used for the resin matrices. Local fiber orientation and length distributions at the key regions on the part are measured for the model validation based on a 15% accuracy criterion. The project outcome will be the ASMI package enhanced with computational capabilities to accurately predict fiber orientation and length distributions in automotive parts designed with long-carbon fiber thermoplastics.

3. Accomplishments

During the first quarter of FY 2016, the following technical progress has been made toward project milestones:

1) Virginia Tech completed fiber orientation (FO) measurements for the samples taken at Locations A, B, C and D (Figure 1) from the 30wt% LCF/PP and 30wt% LCF/PA66 ribbed and non-ribbed complex parts using Virginia Tech's established procedure. Virginia Tech delivered to PNNL all the measured fiber orientation data for validating ASMI fiber orientation predictions.
2) Virginia Tech performed fiber length distribution (FLD) measurements for the samples taken at Locations A, B, C and D from the ribbed complex parts using Virginia Tech's established procedure. Virginia also re-assessed previous data and measured fiber length distributions in the corresponding nozzle purging materials and delivered to PNNL all the measured length data for validating ASMI fiber length predictions.
3) Based on measured fiber orientation data, Autodesk identified the parameters of the anisotropic rotary diffusion reduced strain closure (ARD-RSC) model [1] and provided PNNL with the values of these parameters that were used in ASMI analyses of the complex parts.
4) Magna provided Virginia Tech with additional samples cut out from the 30wt% LCF/PP and 30wt% LCF/PA66 ribbed parts (Figure 1) for fiber length and orientation measurements.
5) In discussion with Autodesk, PNNL performed 3D ASMI analyses of the 30wt% LCF/PP and 30wt% LCF/PA66 ribbed and non-ribbed complex parts to predict fiber orientations and length distributions

in these parts. The issues observed through the analyses regarding fiber orientation distributions profiles and abnormal length distributions were reported to Autodesk. Autodesk is working to resolve these issues.

6) PNNL completed 3D ASMI analyses of the complex parts and compared predicted fiber orientation results at Locations A, B, and C on the non-ribbed parts, and at Locations A, B, C and D on the ribbed parts with the corresponding measured data. PNNL also evaluated the within-15%-agreement criterion using the principal tensile and flexural moduli computed based on predicted vs. measured fiber orientation results.
7) PNNL developed and discussed with Toyota, Magna and PlastiComp a method to perform weight and cost reduction for making the 30wt% LCF/PA66 ribbed part through comparative three-point bending simulations of this part and of similar parts in steel.
8) University of Illinois (Prof. C.L. Tucker) advised the team on fiber orientation and fiber length measurement options, modeling issues as well as interpretation of data.

A bug was discovered in the specification of the inlet profile for fiber length distribution in ASMI. Autodesk has fixed this bug and will provide a new ASMI research version to PNNL. Autodesk continues working on improving the ASMI 3D Fiber solver and works with PNNL to improve fiber orientation predictions for the complex non-ribbed and ribbed parts. PNNL is currently examining the FLD data received from Virginia Tech with Autodesk and the team. The correlations between the predicted and measured FLDs for all the selected locations on the parts will be presented and discussed in the next quarterly report.

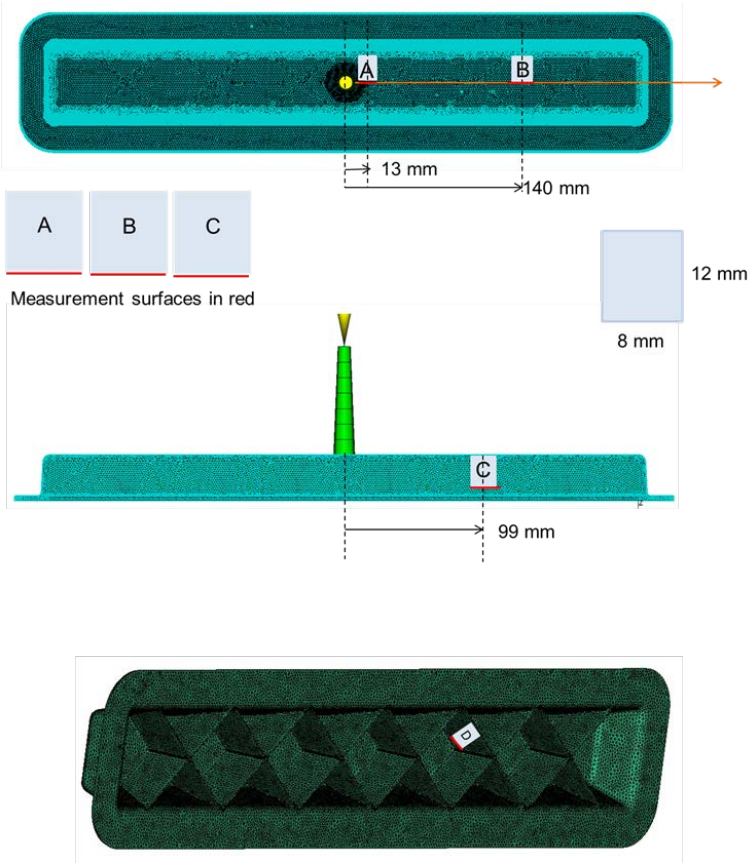

(a)

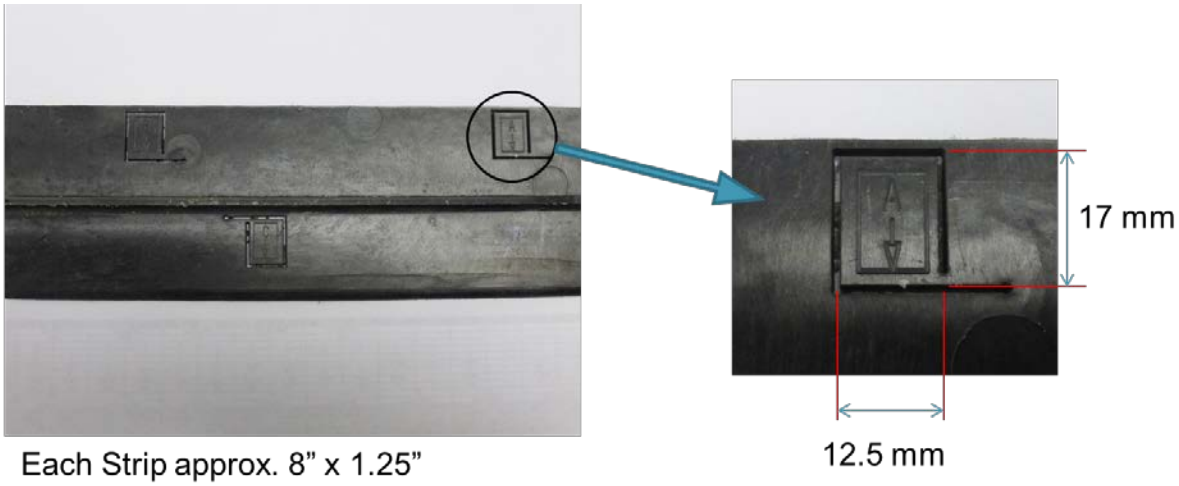

(b)

Figure 1: (a) Locations A, B and C on the ribbed and non-ribbed parts where samples were cut out for fiber orientation and length measurements. Location D is on a rib. The sample size and the measurement surfaces marked in red for fiber orientation measurement are also defined in this figure.

(b) Detailed views of samples before their removals from a complex part.

4. Progress and Status

4.1 Fiber Orientation Measurements for the Ribbed and Non-ribbed Parts (Virginia Tech)

Virginia Tech completed fiber orientation measurements for all the selected samples taken from Locations A, B and C on the non-ribbed parts, and from Locations A, B, C and D on the ribbed parts (Figure 1) processed from the 30wt% LCF/PP and 30wt% LCF/PA66 compounds. The method used by Virginia Tech to measure fiber orientation is presented in our previous report [2]. Figure 2 shows the coordinate system used for all the fiber orientation measurements at Locations A, B, and C. Location D is on a rib (Figure 1). Fiber orientation at Location D was measured and reported in a local coordinate system such that the 1-direction is the thickness direction, the 2-direction points along the width of the rib, and the 3-direction points along the height of the rib (positive direction out of the plane).

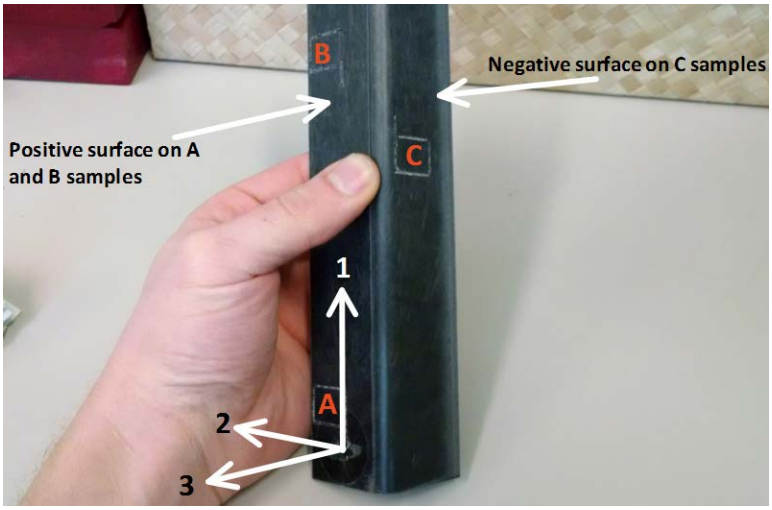

Figure 2. Coordinate system used for all of the FOD measurements at Location A, B and C.

All the measured fiber orientation results are reported and discussed in the next section together with the corresponding ASMI predictions for each location on the ribbed and non-ribbed parts. We have observed different fiber orientation profiles at Location A on the ribbed and non-ribbed part. The measured fiber orientation distribution (FOD) at Location A on the *non-ribbed* 30wt% LCF/PA66 part exhibits the usual shell/core structure while such an orientation structure is significantly less pronounced at Location A on the *ribbed* part made of the same material. In contrast, we have observed the opposite fiber orientation profiles at Location A on the ribbed and non-ribbed parts processed from the 30wt% LCF/PP materials: the FOD at this location on the ribbed part shows the shell/core structure whereas the FOD profile at the same location on the non-ribbed part is relatively flat. The difference in FOD profiles at Location A constitute a significant challenge for fiber orientation predictions.

4.2 Fiber Orientation Predictions for the Ribbed and Non-ribbed Parts (PNNL & Autodesk)

In the last quarter of FY 2015, PNNL worked with Autodesk to build ASMI models for the ribbed and non-ribbed complex parts [2]. PNNL then conducted ASMI analyses of these parts injection molded from the 30wt% LCF/PP and 30wt% LCF/PA66 materials to exercise the models and check part filling. Magna's molding parameters were used in the injection molding simulations of the complex parts (Table 1) [3]. During the first quarter of FY 2016, PNNL performed ASMI analyses of these parts to predict FODs and compare predicted FODs at the selected locations (shown in Figure 1) to the corresponding measured data received from Virginia Tech. Autodesk identified the parameters of the ARD-RSC model based on the fiber orientation data measured from the ribbed and non-ribbed parts processed from these materials. PNNL then used these parameters in trial ASMI analyses and came up a single set of parameters for each material used in the parts. Different options to prescribe the fiber orientation inlet condition in ASMI were tried, and we have found that the option "*fiber aligned at skin/transverse at core*" produced the results that better matched the measured fiber orientation data. The b_i (i=1,…,5) and *RSC* parameters retained for the 30wt% LCF/PP material are:

$$b_1 = 0.0059$$
$$b_2 = 0.01583$$
$$b_3 = -0.01$$
$$b_4 = -0.000418$$
$$b_5 = 0$$
$$RSC = 0.04$$

And those for the 30wt% LCF/PA66 material are:

$$b_1 = 0.04492$$
$$b_2 = -0.4995$$
$$b_3 = 0.56$$
$$b_4 = 0.003066$$
$$b_5 = -0.1$$
$$RSC = 0.02$$

Table 2. Magna LFT molding trial processing conditions for the ribbed and non-ribbed complex parts [3]

Processing Conditions	
Location:	Magna Exteriors and Interiors - Casmir
Machine	Engel 200 TL
Mold	U-Shape Tool
Molding Date	16/17-June-2015

Material	30CF-PA66	30CF-PA66	30CF-PP	30CF-PP
Rib / No-Rib	Ribs	No Ribs	Ribs	No Ribs
Identification Code	30PALR	30PALN	30PPLR	30PPLN
Mold Temp - Cavity	110 C (230 F)	105 C (220 F)	88 C (190 F)	88 C (190 F)
Mold Temp -Core	115 C (240 F)	105 C (220 F)	82 C (180 F)	82 C (180 F)
Melt Temp	320 C (608 F)	320 C (608 F)	248 C (478 F)	248 C (478 F)
Fill Time	2.64 sec	1.93 sec	2.35 sec	2.24 sec
Fill Speed	70 mm/s (2.75 in/sec)	75 mm/s (2.95 in/sec)	60 mm/s (2.36 in/sec)	60 mm/s (2.36 in/sec)
Packing Pressure (Hydraulic)	33 bar (478 psi)	40 bar (580 psi)	28.3 bar (410 psi)	40 bar (580 psi)
Intensification Ratio	9.0	9.0	9.0	9.0
Packing Pressure (Melt)	297 bar (4,308 psi)	360 bar (5,221 psi)	360 bar (5,221 psi)	360 bar (5,221 psi)
Packing time	3.5 sec	5 sec	3 sec	10 sec
Cooling Time	45 sec	45 sec	46 sec	54 sec
Nomimal wall thickness	2.8 mm	2.8 mm	2.8 mm	2.8 mm
Part Weight (with gate)	274 g	233 g	213 g	193 g
Part Weight (without gate)	269 g	228 g	208 g	188 g

The 15% accuracy criterion based on the evaluation of two principal tensile and two principal bending moduli was used to assess the accuracy in fiber orientation prediction for each location on the parts.

4.2.1 Predicted vs. Measured Fiber Orientation Results for the 30wt% LCF/PA66 ribbed part

Figures 3 and 4 report the comparisons between the predicted and measured fiber orientation tensor components A_{11}, A_{22} and A_{33} expressed in the measurement coordinate system (Figure 2) for Locations A and B on the 30wt% LCF/PA66 ribbed part. For these locations, the 1 and 2 directions coincide with the flow and cross flow directions. The measured data for A_{11} and A_{22} at Location A show a very wide core where the orientation state is nearly random with A_{11} and A_{22} fluctuating around 0.5 (Figure 3). The model captures well the variations of A_{11} and A_{22} from the skin to the shell layers at this location but cannot capture the values of these components in the core as the model predicted a very pronounced skin/shell/core orientation structure with fibers aligned in the cross-flow direction in the core. A good agreement between predicted and measured A_{33} is observed at Location A. The model, however, provides better predictions for A_{11} and A_{22} at Location B as reported in Figure 4 that shows globally good agreements between predicted and experimental results although the model cannot completely capture the core. In contrast to the fiber orientation profile at Location A, the measured fiber orientation data at Location B clearly exhibit the usual skin/shell/core structure. Figure 5 presents the predicted fiber orientation results that are seen to compare well to the measured data for Location C on this part. The measured fiber orientation profile exhibits high alignment in the 1-direction that is very well captured by the model. Good agreement of results is found for all three components of the orientation tensor.

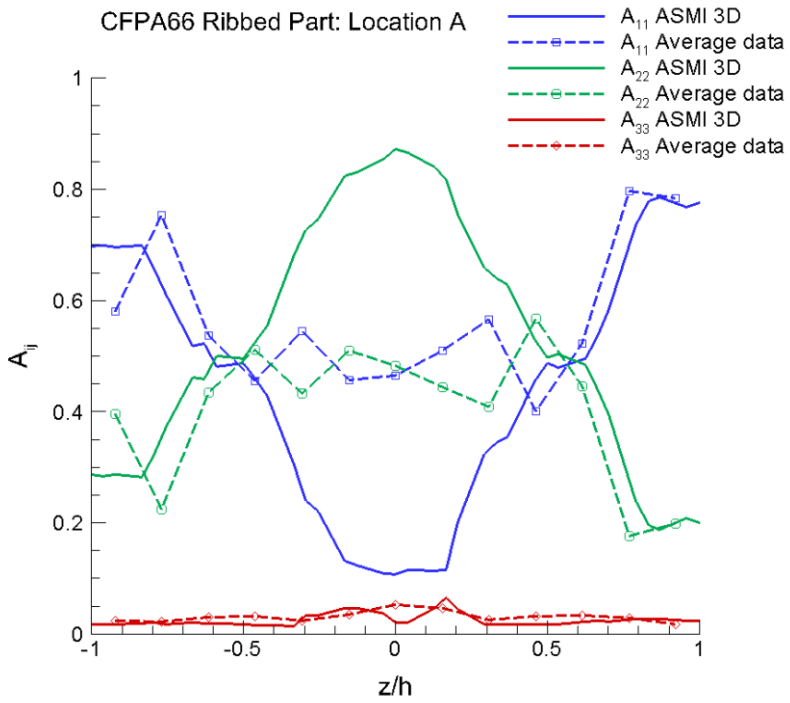

Figure 3. Predictions vs. measured data for the fiber orientation tensor components A_{11}, A_{22} and A_{33} for Location A on the 30wt% LCF/PA66 ribbed part. *z/h* denotes the normalized *z* coordinate with *h* being the half of the sample thickness.

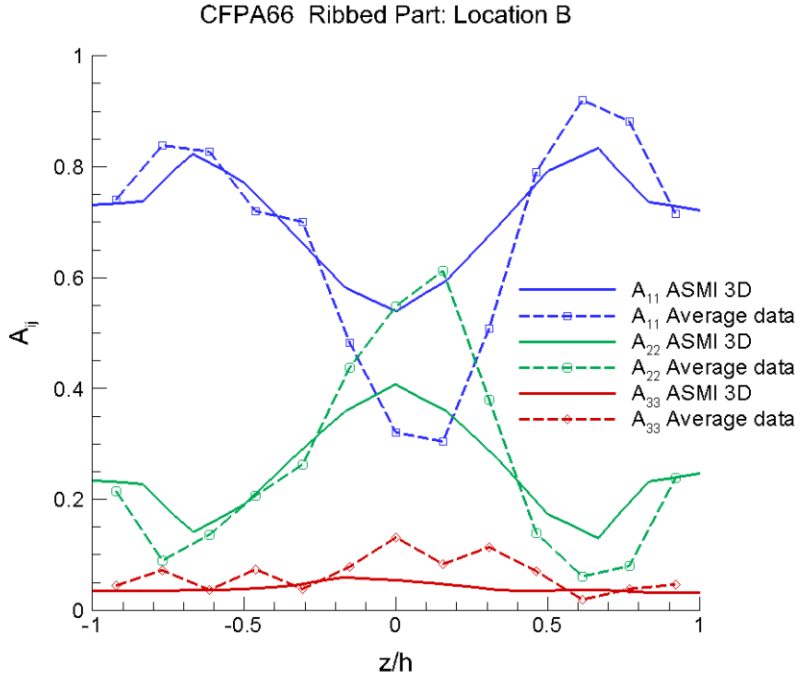

Figure 4. Predictions vs. measured data for the fiber orientation tensor components A_{11}, A_{22} and A_{33} for Location B on the 30wt% LCF/PA66 ribbed part.

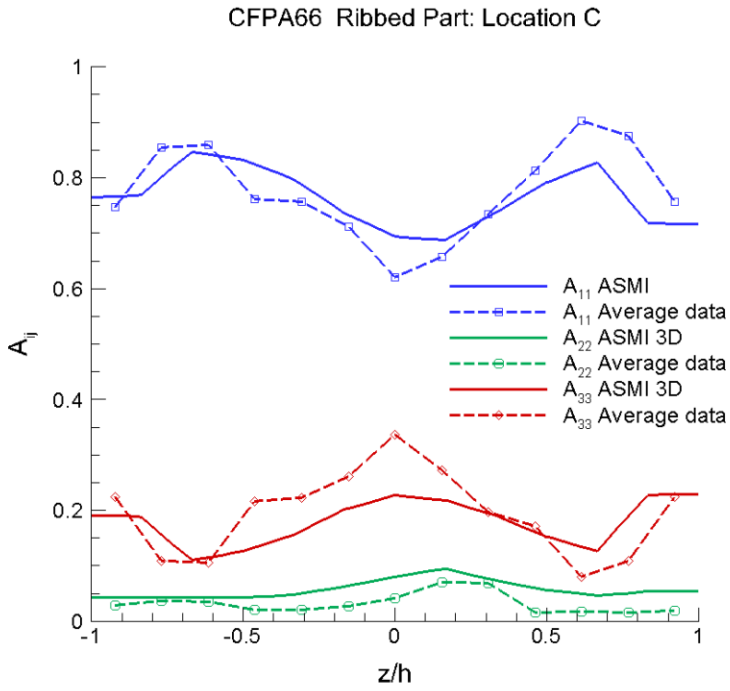

Figure 5. Predictions vs. measured data for the fiber orientation tensor components A_{11}, A_{22} and A_{33} for Location C on the 30wt% LCF/PA66 ribbed part.

Figure 6 reports the fiber orientation predictions for Location D (on a rib) compared to the measured data at this location. As mentioned earlier, the measurement coordinate used for Location D is such that the 1-direction is the thickness direction, the 2-direction points along the width of the rib, and the 3-direction points along the height of the rib (positive direction out of the plane). ASMI fiber orientation results obtained in the structural XYZ axes were then expressed in the measurement coordinate system for comparison of results reported in Figure 6. There are global agreements between the predicted and measured results for A_{22} and A_{33}. The model roughly captures the nearly random fiber orientation distribution in the 2-3 plane, however, it largely over-predicted A_{11} for the values of the normalized thickness z/h between -0.5 and 1.

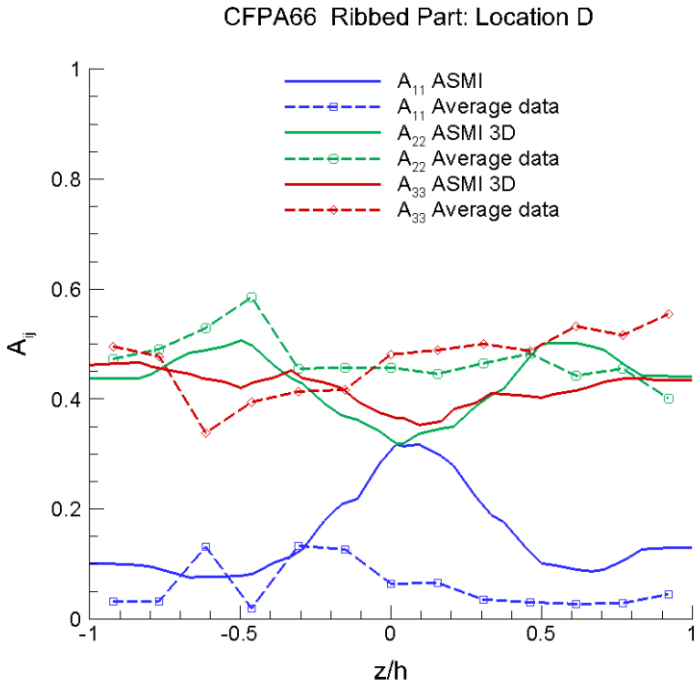

Figure 6. Predictions vs. measured data for the fiber orientation tensor components A_{11}, A_{22} and A_{33} for Location D on the 30wt% LCF/PA66 ribbed part.

Tables 1 to 4 provide the tensile and flexural moduli calculated based on the predicted and measured fiber orientations for all the selected locations on the 30wt% LCF/PA66 ribbed part. The computation of elastic moduli assumed typical elastic properties of the carbon fiber and of the thermoplastic matrices (PP and PA66). The following values were used for the elastic properties of the carbon fiber: longitudinal elastic modulus, E_L = 230 GPa, transverse elastic modulus, E_T = 13.8 GPa, longitudinal shear modulus, G_L = 12.4 GPa, longitudinal Poisson's ratio, ν_L = 0.2, and transverse Poisson's ratio ν_T = 0.25. The assumed elastic modulus and Poisson's ratio of PP were 1.7 GPa and 0.4; and those for PA66 were 3.3 GPa and 0.35, respectively. A uniform fiber aspect ratio, *l/d* = 200 was also assumed in the computation. The method to compute the tensile and flexural moduli is given in [4].

Table 1 shows that the 15% accuracy criterion was not met at Location A for E_{11} and E_{22}. This was due to the large model under-prediction for A_{11} and over-prediction for A_{22} (Figure 3). However, better correlations between predicted and measured FODs at Locations B and C (Figures 4 and 5) have led the predictions of all the elastic moduli to be with 15% of the measured data (Tables 2 and 3). For Location D (Table 4), the accuracy criterion was not met for E_{22} and E_{33}, but the exceedances were rather small.

Table 1. Computed tensile moduli E_{11} and E_{22}, and flexural moduli D_{11} and D_{22} based on measured and predicted fiber orientations at Location A on the 30wt% LCF/PA66 ribbed part.

Modulus (Location A)	Using Predicted Fiber Orientation	Using Measured Fiber Orientation	Agreement within
E_{11} (MPa)	21134	25568	17.3%
E_{22} (MPa)	24539	17585	39.5%
D_{11} (MPa.mm^3)	61510	62631	1.79%
D_{22} (MPa.mm^3)	34181	32747	4.38%

Table 2. Computed tensile moduli E_{11} and E_{22}, and flexural moduli D_{11} and D_{22} based on measured and predicted fiber orientations at Location B on the 30wt% LCF/PA66 ribbed part.

Modulus (Location B)	Using Predicted Fiber Orientation	Using Measured Fiber Orientation	Agreement within
E_{11} (MPa)	33249	32268	3.04%
E_{22} (MPa)	11795	12604	6.42%
D_{11} (MPa.mm^3)	73694	77610	5.05%
D_{22} (MPa.mm^3)	23568	20687	13.9%

Table 3. Computed tensile moduli E_{11} and E_{33}, and flexural moduli D_{11} and D_{33} based on measured and predicted fiber orientations at Location C on the 30wt% LCF/PA66 ribbed part.

Modulus (Location C)	Using Predicted Fiber Orientation	Using Measured Fiber Orientation	Agreement within
E_{11} (MPa)	36280	37149	2.34%
E_{33} (MPa)	8672	9982	13.1%
D_{11} (MPa.mm^3)	76774	80489	4.62%
D_{33} (MPa.mm^3)	20509	20754	1.18%

Table 4. Computed tensile moduli E_{22} and E_{33}, and flexural moduli D_{22} and D_{33} based on measured and predicted fiber orientations at Location D on the 30wt% LCF/PA66 ribbed part.

Modulus (Location D)	Using Predicted Fiber Orientation	Using Measured Fiber Orientation	Agreement within
E_{22} (MPa)	16812	19849	15.3%
E_{33} (MPa)	16390	20009	18.1%
D_{22} (MPa.mm^3)	3760	3977	5.46%
D_{33} (MPa.mm^3)	3641	4183	13.0%

4.2.2 Predicted vs. Measured Fiber Orientation Results for the 30wt% LCF/PA66 Non-ribbed part

Figures 7, 8 and 9 present the comparisons between the predicted and measured fiber orientation tensor components A_{11}, A_{22} and A_{33} for Locations A, B and C on the 30wt% LCF/PA66 non-ribbed part, respectively. There is good global agreement between predicted and experimental results for all the components at Location A. For Location B, although the model roughly captured the through-thickness variations of A_{11} and A_{22}, it significantly overpredicts A_{11} and under-predicts A_{22} in the core (Figure 8). The same result was found for Location C (Figure 9): the model captured the general trends but significantly over-predicted A_{11} and A_{22}, and underpredicted A_{33}.

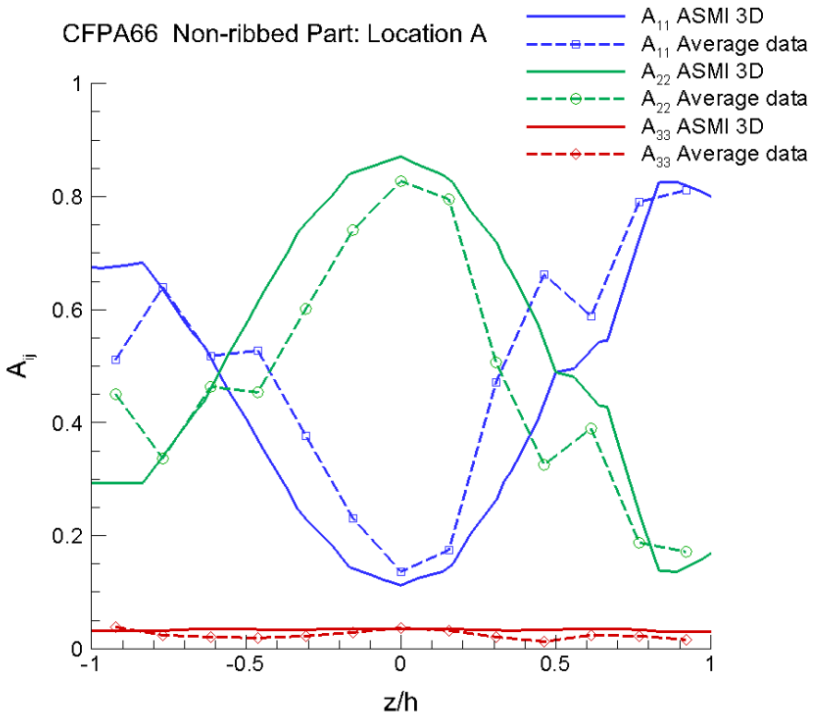

Figure 7. Predictions vs. measured data for the fiber orientation tensor components A_{11}, A_{22} and A_{33} for Location A on the 30wt% LCF/PA66 non-ribbed part.

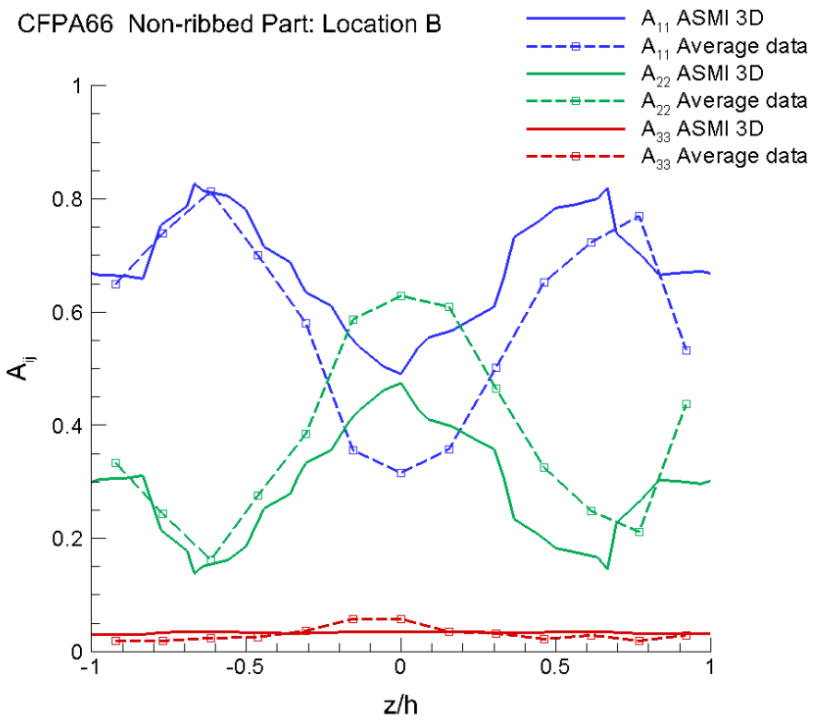

Figure 8. Predictions vs. measured data for the fiber orientation tensor components A_{11}, A_{22} and A_{33} for Location B on the 30wt% LCF/PA66 non-ribbed part.

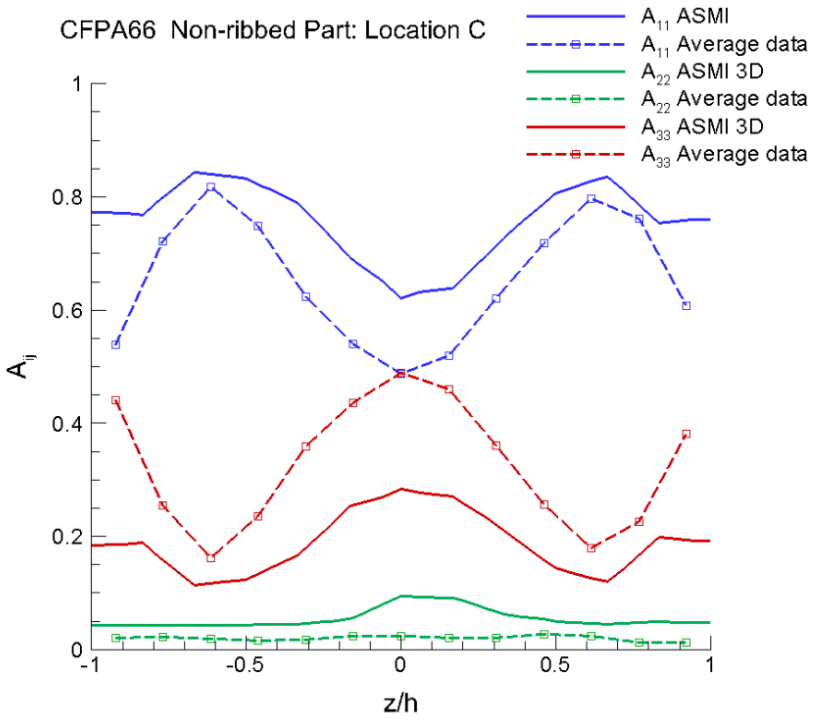

Figure 9. Predictions vs. measured data for the fiber orientation tensor components A_{11}, A_{22} and A_{33} for Location C on the 30wt% LCF/PA66 non-ribbed part.

Tables 5 to 7 report the tensile and flexural moduli calculated based on the predicted and measured fiber orientations for all the selected locations on the 30wt% LCF/PA66 non-ribbed part. Table 5 shows that the 15% accuracy criterion is met at Location A for all the moduli except for E_{22} but the exceedance is small. The criterion is not met at Location B for E_{11} and E_{22} due to the significant over-prediction of A_{11} and underprediction of A_{22} for this location (Figure 8). The substantial overpredictions of A_{11} and A_{22} as well as the substantial underprediction for A_{33} (Figure 9) are responsible for the large exceedances of the criterion for all the moduli at Location C (Table 7).

Table 5. Computed tensile moduli E_{11} and E_{22}, and flexural moduli D_{11} and D_{22} based on measured and predicted fiber orientations at Location A on the 30wt% LCF/PA66 non-ribbed part.

Modulus (Location A)	Using Predicted Fiber Orientation	Using Measured Fiber Orientation	Agreement within
E_{11} (MPa)	20721	23140	10.5%
E_{22} (MPa)	25897	21957	17.9%
D_{11} (MPa.mm^3)	61436	61308	2.09%
D_{22} (MPa.mm^3)	33993	33993	0%

Table 6. Computed tensile moduli E_{11} and E_{22}, and flexural moduli D_{11} and D_{22} based on measured and predicted fiber orientations at Location B on the 30wt% LCF/PA66 non-ribbed part.

Modulus (Location B)	Using Predicted Fiber Orientation	Using Measured Fiber Orientation	Agreement within
E_{11} (MPa)	31555	26616	18.6%
E_{22} (MPa)	13191	17064	22.7%
D_{11} (MPa.mm^3)	68929	64656	6.61%
D_{22} (MPa.mm^3)	26844	30753	12.7%

Table 7. Computed tensile moduli E_{11} and E_{33}, and flexural moduli D_{11} and D_{33} based on measured and predicted fiber orientations at Location C on the 30wt% LCF/PA66 non-ribbed part.

Modulus (Location C)	Using Predicted Fiber Orientation	Using Measured Fiber Orientation	Agreement within
E_{11} (MPa)	35106	30029	16.9%
E_{33} (MPa)	8875	14580	39.1%
D_{11} (MPa.mm^3)	79000	67106	17.7%
D_{33} (MPa.mm^3)	20696	31345	34.0%

4.2.3 Predicted vs. Measured Fiber Orientation Results for the 30wt% LCF/PP Ribbed Part

Figures 10, 11, 12 and 13 show the comparisons between the predicted and measured fiber orientation tensor components A_{11}, A_{22} and A_{33} for Locations A, B, C and D on the 30wt% LCF/PP ribbed part, respectively. The model captures very well the thru-thickness FOD profile at Location A where very good correlations between the predicted and measured fiber orientations for all the components are found (Figure 10). At Location B, although the model generally captures the core and the variation trends for all three components, it significantly underpredicts the values of A_{11} and over-predicts A_{22} in the shell layers (Figure 11). Figure 12 shows very good agreement of results at Location C for all the components. In the previous section, we have also observed good correlations of results at Location C on the 30wt% LCF/PA66 ribbed part (Figure 5). Predicted FOD results compared to the measured FOD data for Location D are reported in Figure 13 that shows a nearly random FOD profile in the 2-3 plane. The model can only roughly capture the order of magnitude of A_{11} and A_{22} but significantly over-predicts A_{33}. Tables 8 to 11 provide the tensile and flexural moduli calculated based on the predicted and measured fiber orientations for all the selected locations on the 30wt% LCF/PP ribbed part. Good correlations between the predicted and measured FODs at Locations A (Figure 10) and C (Figure 12) have produced good agreements between the moduli computed using the predicted FODs and those computed using the measured FODs at these locations (Tables 8 and 10). However, the accuracy criterion is neither met at Location B for all the moduli nor at Location D for E_{22}, D_{22} and D_{33}. The mismatches between predicted and measured FODs discussed above do not yield the agreement of moduli within 15%.

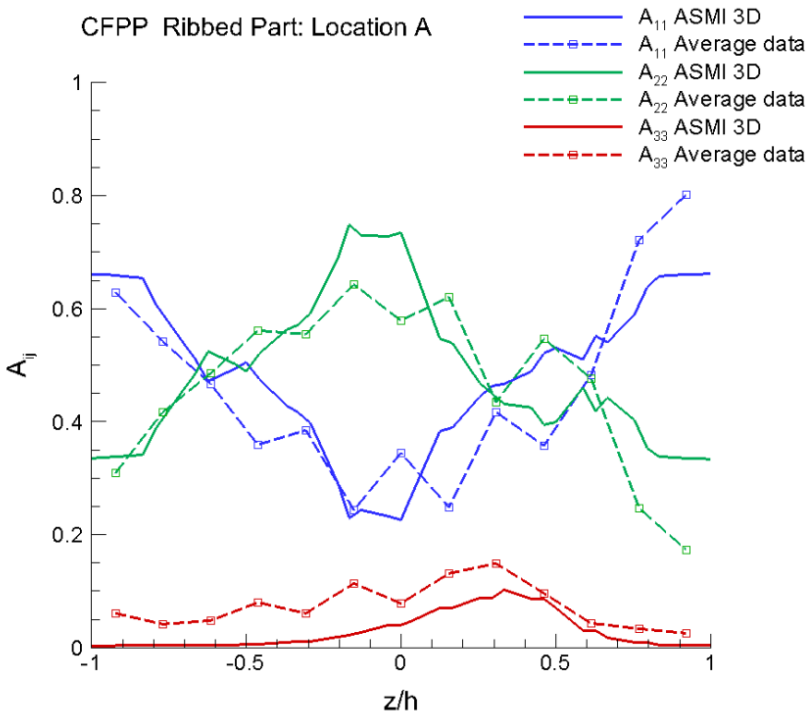

Figure 10. Predictions vs. measured data for the fiber orientation tensor components A_{11}, A_{22} and A_{33} for Location A on the 30wt% LCF/PP ribbed part.

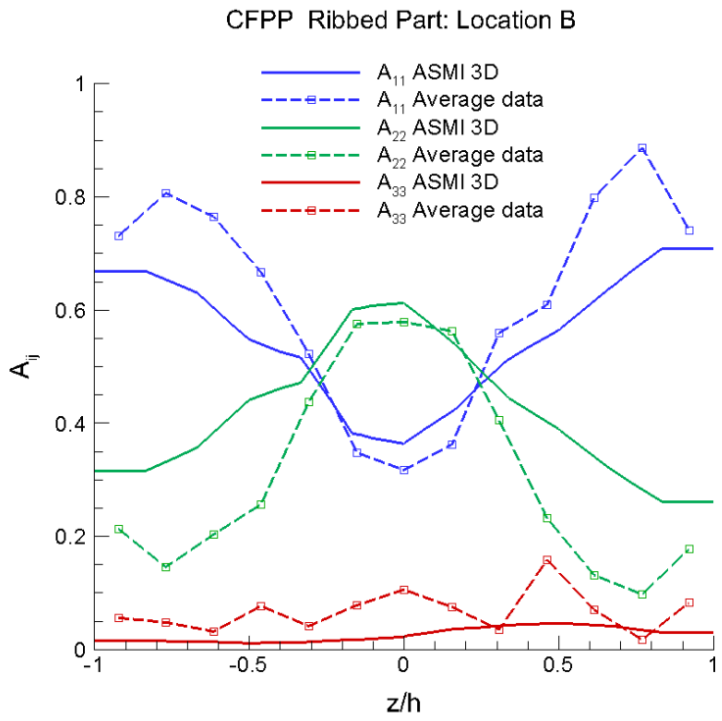

Figure 11. Predictions vs. measured data for the fiber orientation tensor components A_{11}, A_{22} and A_{33} for Location B on the 30wt% LCF/PP ribbed part.

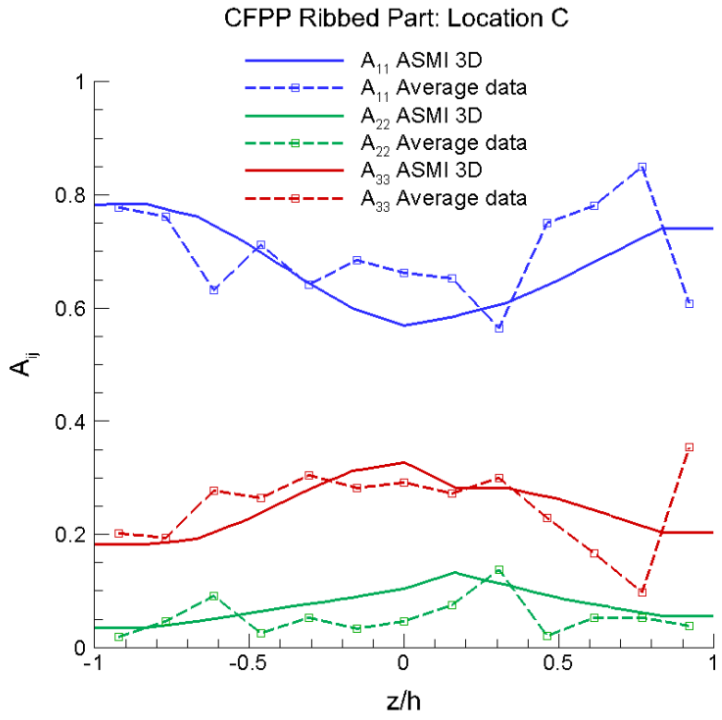

Figure 12. Predictions vs. measured data for the fiber orientation tensor components A_{11}, A_{22} and A_{33} for Location C on the 30wt% LCF/PP ribbed part.

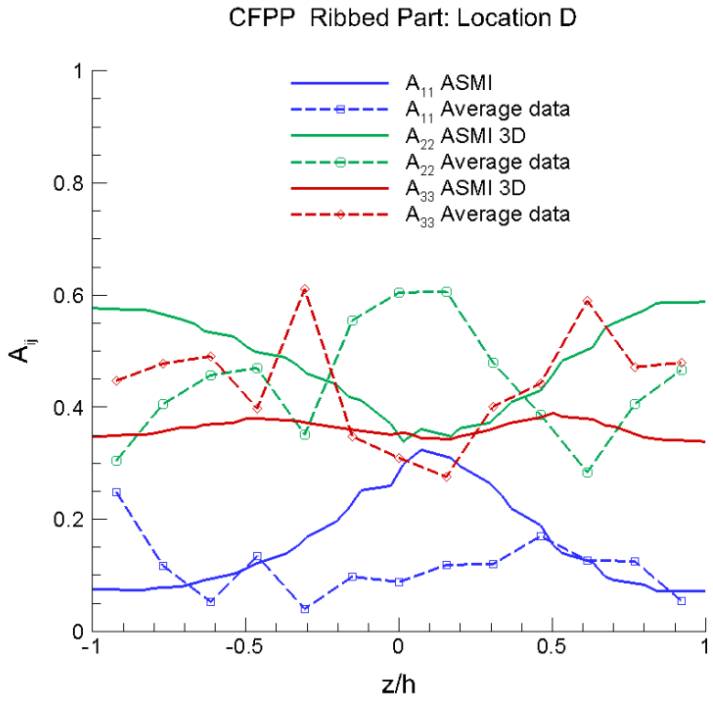

Figure 13. Predictions vs. measured data for the fiber orientation tensor components A_{11}, A_{22} and A_{33} for Location D on the 30wt% LCF/PP ribbed part.

Table 8. Computed tensile moduli E_{11} and E_{22}, and flexural moduli D_{11} and D_{22} based on measured and predicted fiber orientations at Location A on the 30wt% LCF/PP ribbed part.

Modulus (Location A)	Using Predicted Fiber Orientation	Using Measured Fiber Orientation	Agreement within
E_{11} (MPa)	17002	15764	7.85%
E_{22} (MPa)	16749	15751	6.34%
D_{11} (MPa.mm^3)	46395	46426	0.07%
D_{22} (MPa.mm^3)	29969	27489	9.02%

Table 9. Computed tensile moduli E_{11} and E_{22}, and flexural moduli D_{11} and D_{22} based on measured and predicted fiber orientations at Location B on the 30wt% LCF/PP non-ribbed part

Modulus (Location B)	Using Predicted Fiber Orientation	Using Measured Fiber Orientation	Agreement within
E_{11} (MPa)	19443	22976	15.4%
E_{22} (MPa)	14305	10527	35.9%
D_{11} (MPa.mm^3)	50585	60690	16.7%
D_{22} (MPa.mm^3)	25426	16658	52.6%

Table 10. Computed tensile moduli E_{11} and E_{33}, and flexural moduli D_{11} and D_{33} based on measured and predicted fiber orientations at Location C on the 30wt% LCF/PP ribbed part.

Modulus (Location C)	Using Predicted Fiber Orientation	Using Measured Fiber Orientation	Agreement within
E_{11} (MPa)	24292	25337	4.12%
E_{33} (MPa)	7608	7965	4.48%
D_{11} (MPa.mm^3)	58214	58152	0.11%
D_{33} (MPa.mm^3)	17542	19065	7.80%

Table 11. Computed tensile moduli E_{22} and E_{33}, and flexural moduli D_{22} and D_{33} based on measured and predicted fiber orientations at Location D on the 30wt% LCF/PP ribbed part.

Modulus (Location D)	Using Predicted Fiber Orientation	Using Measured Fiber Orientation	Agreement within
E_{22} (MPa)	14468	13645	6.03%
E_{33} (MPa)	10601	13669	22.4%
D_{22} (MPa.mm^3)	3716	2645	40.5%
D_{33} (MPa.mm^3)	2358	3197	26.2%

4.2.4 Predicted vs. Measured Fiber Orientation Results for the 30wt% LCF/PP Non-ribbed Part

Figures 14, 15, and 16 compare the predicted to measured fiber orientation tensor components A_{11}, A_{22} and A_{33} for Locations A, B, and C on the 30wt% LCF/PP non-ribbed part, respectively. As mentioned earlier, the experimental FOD profile at Location A on this part is relatively "flat" and does not exhibit the usual skin/shell/core layered structure. This kind of profile constitutes a significant challenge for the ARD-RSC model as this model predicts a skin/shell/core layered structure near the gate and at the downstream positions along the flow direction and on the same surface. As a result, the predicted FOD cannot match the measured FOD at Location A (Figure 14). Autodesk is working on remedying this problem. The model, however, predicts well the FOD at Location B whose FOD profile displays the usual fiber orientation structure (Figure 15). The model reasonably predicts A_{11} at Location C but the quite large underprediction of A_{33} led to over-predicting A_{22}.

Tables 12 to 14 provide the tensile and flexural moduli calculated based on the predicted and measured fiber orientations for all the selected locations on this part. Good match between the predicted and measured FODs at Location B has produced excellent agreements of moduli results. However, the mismatches between predicted and measured FODs as discussed above have led to large exceedances of the criterion for E_{22} at Location A as well as for E_{33} and D_{33} at Location C.

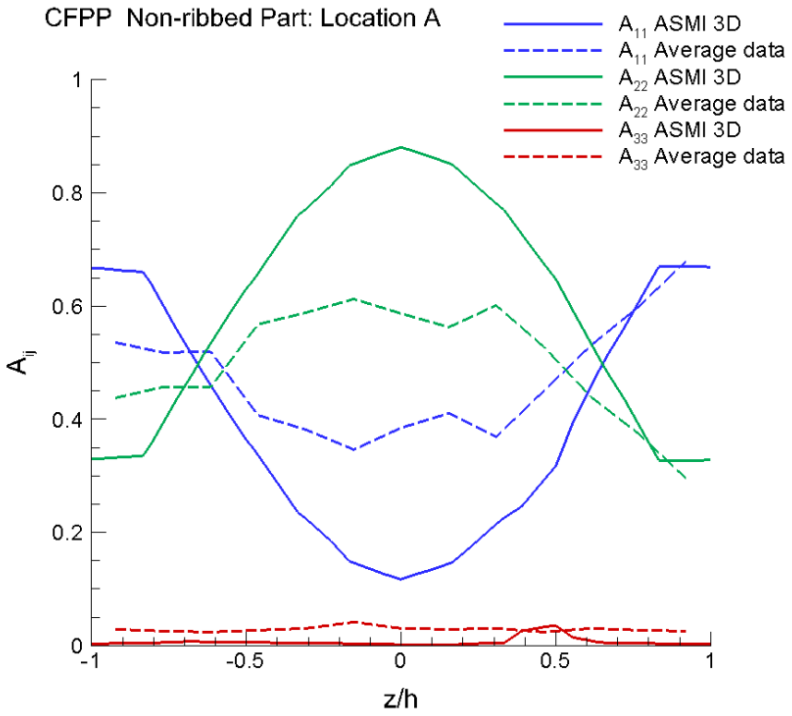

Figure 14. Predictions vs. measured data for the fiber orientation tensor components A_{11}, A_{22} and A_{33} for Location A on the 30wt% LCF/PP non-ribbed part.

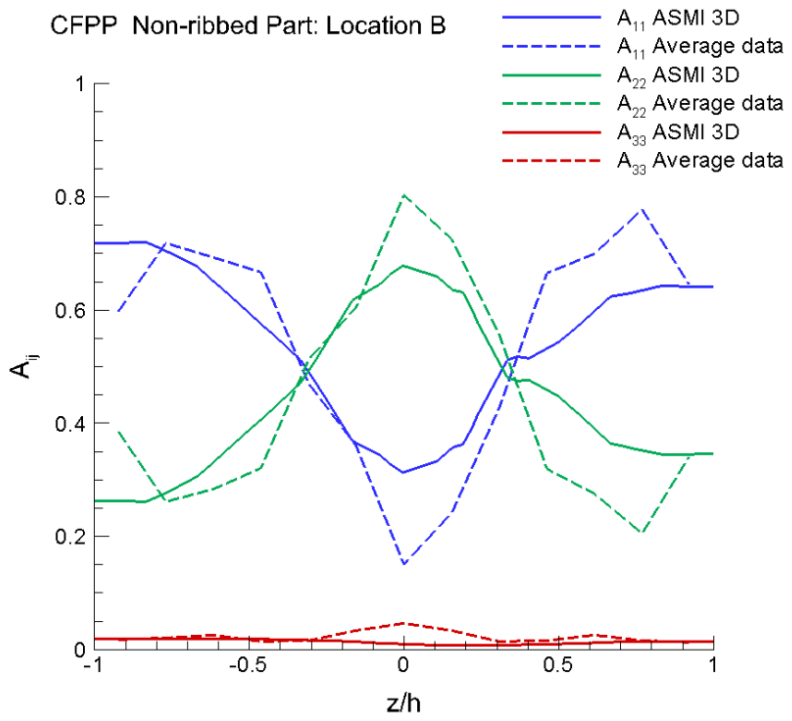

Figure 15. Predictions vs. measured data for the fiber orientation tensor components A_{11}, A_{22} and A_{33} for Location B on the 30wt% LCF/PP non-ribbed part.

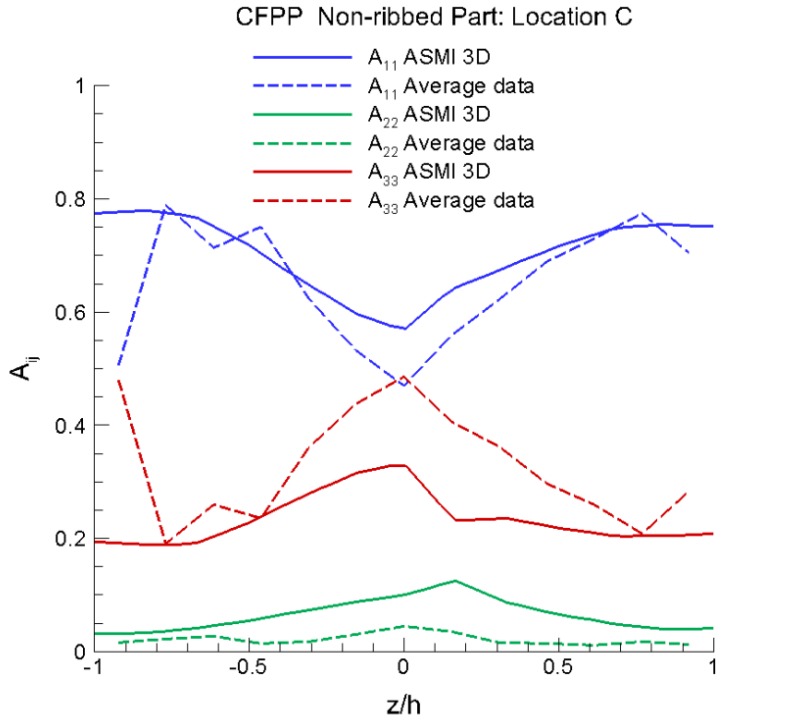

Figure 16. Predictions vs. measured data for the fiber orientation tensor components A_{11}, A_{22} and A_{33} for Location C on the 30wt% LCF/PP non-ribbed part.

Table 12. Computed tensile moduli E_{11} and E_{22}, and flexural moduli D_{11} and D_{22} based on measured and predicted fiber orientations at Location A on the 30wt% LCF/PP non-ribbed part.

Modulus (Location A)	Using Predicted Fiber Orientation	Using Measured Fiber Orientation	Agreement within
E_{11} (MPa)	14535	15116	3.84%
E_{22} (MPa)	22868	15657	46.1%
D_{11} (MPa.mm^3)	44589	41866	6.50%
D_{22} (MPa.mm^3)	33003	31977	3.21%

Table 13. Computed tensile moduli E_{11} and E_{22}, and flexural moduli D_{11} and D_{22} based on measured and predicted fiber orientations at Location B on the 30wt% LCF/PP non-ribbed part.

Modulus (Location B)	Using Predicted Fiber Orientation	Using Measured Fiber Orientation	Agreement within
E_{11} (MPa)	19509	19948	2.20%
E_{22} (MPa)	15244	15076	1.11%
D_{11} (MPa.mm^3)	50708	52142	2.75%
D_{22} (MPa.mm^3)	26210	24913	5.21%

Table 14. Computed tensile moduli E_{11} and E_{22}, and flexural moduli D_{11} and D_{22} based on measured and predicted fiber orientations at Location C on the 30wt% LCF/PP non-ribbed part.

Modulus (Location C)	Using Predicted Fiber Orientation	Using Measured Fiber Orientation	Agreement within
E_{11} (MPa)	25630	23197	10.50%
E_{33} (MPa)	7065	10510	32.80%
D_{11} (MPa.mm^3)	60132	54467	10.40%
D_{33} (MPa.mm^3)	17015	23636	28.0%

5. Publications/Presentations

None

6. Patents

None

7. Future Plans

PNNL will continue working with Autodesk to improve fiber orientation predictions for the complex ribbed and non-ribbed parts upon receiving a new research version of ASMI with the improved 3D Fiber solver. Upon receipt of a new ASMI version, PNNL will re-analyze the complex parts to predict fiber length distributions at all the selected locations. Predicted FLDs will be compared with measured FLDs to validate the fiber length model. Finally, while exploring and refining ASMI results, PNNL will continue working with Toyota to perform weight and cost saving studies for the complex ribbed 30wt% LCF/PA66 part. Three-point bending simulations of the composite part and of the non-ribbed parts in steel will be completed, and analysis results will be used in the design of the composite part to meet the weight and cost reduction targets. A cost study to compare the weight and cost benefits of LCF/PA66 vs. traditional stamped steel for structural automotive parts is being evaluated with Magna to provide cost and weight estimates for the composite part using 30wt% LCF/PA66, 40wt% LCF/PA66, 50wt% LCF/PA66 and 40wt% long-glass-fiber/PA66.

8. References

[1] Phelps JH and Tucker III CL (2009). An Anisotropic Rotary Diffusion Model for Fiber Orientation in Short- and Long-Fiber Thermoplastics, Journal of the Non-Newtonian Fluid Mechanics, 156(3):165-176.
[2] Nguyen, B.N.; Fifield, L.S.; Roland, D.; Wollan, E.J.; Gandhi, U.N.; Mori, S.; Gregory, L.; Baird, D.G.; Wang, J.; Franco, C.; Tucker III, C.L. (2015). Predictive Engineering Tools for Injection-Molded Long-Carbon-Fiber Thermoplastic Composites – FY 2015 Fourth Quarterly Report; PNNL-24834; Pacific Northwest National Laboratory, Richland, WA.
[3] Nguyen, B.N.; Fifield, L.S.; Mori, S.; Gandhi, U.N.; Wang, J.; Franco, C.; Wollan, E.J.; Tucker III, C.L. (2015 c). Predictive Engineering Tools for Injection-Molded Long-Carbon-Fiber Thermoplastic Composites – FY 2015 Third Quarterly Report; PNNL-24472; Pacific Northwest National Laboratory, Richland, WA.
[4] Nguyen, B.N.; Fifield, L.S.; Mathur, R.N.; Kijewski , S.A.; Sangid, M.D.; Wang, J.; Franco, C.; Gandhi, U.N.; Mori, S.; Tucker III, C.L. (2015). Predictive Engineering Tools for Injection-Molded Long-Carbon-Fiber Thermoplastic Composites – FY 2014 Fourth Quarterly Report; PNNL-23842; Pacific Northwest National Laboratory, Richland, WA.

9. Budgetary Information

Baseline Reporting Quarter	Budget Period 2											
	FY15-Q2		FY15-Q3		FY15-Q4		FY16-Q1		FY16-Q2		FY16-Q3	
	1/1/2015 - 3/31/2015		4/1/2015 - 6/30/2015		7/1/2015 - 9/30/2015		10/1/15 - 12/31/2015		1/1/2016 - 3/31/2016		4/1/2016 - 6/30/2016	
	Q2	Cumulative Total	Q3	Cumulative Total	Q4	Cumulative Total	Q1	Cumulative Total	Q2	Cumulative Total	Q3	Cumulative Total
Baseline Cost Plan												
Federal Share	$101,927	$593,312	$56,013	$649,325	$117,232	$766,557	$117,232	$883,788	$58,616	$942,404	$58,616	$1,001,020
Non-Federal Share	$102,294	$672,648	$102,294	$774,941	$102,294	$877,235	$102,294	$979,528	$51,147	$1,030,675	$51,147	$1,081,822
Total Planned	$204,221	$1,265,960	$158,307	$1,424,266	$219,525	$1,643,791	$219,525	$1,863,317	$109,763	$1,973,080	$109,763	$2,082,842
Actual Incurred Cost												
Federal Share	$71,374	$588,765	$58,637	$647,402	$84,981	$732,384	$94,284	$826,668		$826,668		$826,668
Non-Federal Share	$127,783	$1,083,395	$135,147	$1,218,542	$92,282	$1,310,824	$53,907	$1,364,731		$1,364,731		$1,364,731
Total Incurred Costs	$199,157	$1,672,160	$193,784	$1,865,945	$177,264	$2,043,208	$148,191	$2,191,399		$2,191,399		$2,191,399
Variance												
Federal Share	$30,553	$4,547	-$2,624	$1,923	$32,250	$34,173	$22,948	$57,121				
Non-Federal Share	-$25,489	-$410,748	-$32,853	-$443,601	$10,012	-$433,590	$48,387	-$385,203				
Total Variance	$5,064	-$406,201	-$35,478	-$441,678	$42,262	-$399,417	$71,334	-$328,082				

Pacific Northwest
NATIONAL LABORATORY

Proudly Operated by **Battelle** *Since 1965*

U.S. DEPARTMENT OF
ENERGY

902 Battelle Boulevard
P.O. Box 999
Richland, WA 99352
1-888-375-PNNL (7665)

www.pnnl.gov